energies

MDPI

Article

Optimization of Ampacity in High-Voltage Underground Cables with Thermal Backfill Using Dynamic PSO and Adaptive Strategies

Brayan A. Atoccsa [1,*], David W. Puma [2], Daygord Mendoza [1], Estefany Urday [3], Cristhian Ronceros [3] and Modesto T. Palma [1]

[1] Faculty of Mechanical Engineering, National University of Engineering, Lima 15333, Peru; dmendozaro@uni.pe (D.M.); mpalmag@uni.edu.pe (M.T.P.)
[2] Faculty of Electrical and Power Engineering, Technological University of Peru, Lima 15306, Peru; dpumat@uni.pe
[3] Faculty of Engineering, Private University San Juan Bautista, Ica 11004, Peru; estefany.urday@autonomadeica.edu.pe (E.U.); cristhian.ronceros@autonomadeica.edu.pe (C.R.)
* Correspondence: bryan.atoccsa@gmail.com

Abstract: This article addresses challenges in the design of underground high-voltage transmission lines, focusing on thermal management and cable ampacity determination. It introduces an innovative proposal that adjusts the dimensions of the backfill to enhance ampacity, contrasting with the conventional approach of increasing the core cable's cross-sectional area. The methodology employs a particle swarm optimization (PSO) technique with adaptive penalization and restart strategies, implemented in MATLAB for parameter autoadaptation. The article emphasizes more efficient solutions than traditional PSO, showcasing improved convergence and precise results (success probability of 66.1%). While traditional PSO is 81% faster, the proposed PSO stands out for its accuracy. The inclusion of thermal backfill results in an 18.45% increase in cable ampacity, considering variations in soil thermal resistivity, backfill properties, and ambient temperature. Additionally, a sensitivity analysis was conducted, revealing conservative values that support the proposal's robustness. This approach emerges as a crucial tool for underground installation, contributing to continuous ampacity improvement and highlighting its impact on decision making in energy systems.

Keywords: underground transmission; high voltage; thermal management; cable ampacity; thermal backfill; PSO; adaptive penalization; sensitivity analysis

Citation: Atoccsa, B.A.; Puma, D.W.; Mendoza, D.; Urday, E.; Ronceros, C.; Palma, M.T. Optimization of Ampacity in High-Voltage Underground Cables with Thermal Backfill Using Dynamic PSO and Adaptive Strategies. *Energies* **2024**, *17*, 1023. https://doi.org/10.3390/en17051023

Academic Editors: Lin Zhu and Zhigang Wu

Received: 11 January 2024
Revised: 10 February 2024
Accepted: 18 February 2024
Published: 22 February 2024

1. Introduction

As population density continues to rise, the demand for electrical energy experiences significant growth. In response to this challenge, electric companies are constantly seeking innovations to enhance the ampacity of their transmission and distribution systems to meet the growing demand. In densely populated environments, underground transmission lines emerge as the preferred option due to their easier installation compared to traditional overhead lines.

The ampacity of power cables is primarily based on the cross-sectional area of the conductor core, making it crucial to evaluate this parameter to meet specifications [1]. This aspect has been extensively addressed in the literature and governed by international standards, such as those established by IEEE and IEC [2–4]. Analytical methods supported by these organizations, based on the model proposed by Neher and McGrath [5], are commonly used to calculate the ampacity of power cables.

Over time, various specialized software tools have been developed to calculate ampacity in different cable configurations, taking into account various soil layers and installation conditions. Examples include programs like CYMCAP [6–8], ETAP [9], and COMSOL [10].

The history of ampacity calculations is extensively documented in the literature, detailing various factors affecting cable ampacity [2,6].

Ampacity has been found to be closely linked to installation conditions and material properties [6,11,12]. Soil thermal resistivity, in particular, is crucial in the thermal analysis of cables [13]. It is estimated that over 70% of the temperature increase in buried cables is attributed to external thermal resistance [2,13]. A common practice to enhance heat dissipation capacity and, consequently, cable ampacity, is the use of backfill [2,14–16]. Although this practice is effective in high-resistivity soils or under dry soil and low-temperature conditions [2,6], its application can be costly, especially in urban areas with space limitations [17]. From an economic perspective, adjusting the backfill proves to be a more cost-effective alternative than increasing the core size of high-voltage cables, as it directly impacts costs [1]. Despite associated costs, the application of backfill is essential to extend the cable's lifespan, making it crucial to optimize its configuration and installation dimensions to achieve optimal ampacity at a reasonable cost.

Various mathematical models and algorithms have been developed to optimize cable ampacity and installation dimensions in different configurations. In [18], a model is presented that selects the optimal cross-sectional area of the conductor and the corrective dimension of the backfill. Additionally, the authors of [16] propose a methodology to optimize the thermal performance of power cables based on configuration parameters. Research has also explored the impact of controlled backfill quantity on native soil thermal resistivity [13,19] and the ampacity of high-voltage cables in relation to cable spacing, burial depth, and backfill size [20–22]. Recent studies, such as those by [23,24], have employed algorithms like PSO, Jaya, MJaya, and NSGA-III for multi-objective optimization, ranging from backfill cost minimization to improving the thermal environment in underground lines. In [25], the calculation and analysis method of cable ampacity in a ductbank is studied using the NSGA-III algorithm for multi-objective optimization, while [26] uses the grey wolf optimization algorithm to enhance ampacity, achieving an optimal design of high-voltage cable layout in tunnels. Although ampacity optimization has advanced with the use of various algorithms in different contexts, it is crucial to note that it remains an evolving research area, especially in the field of underground cables.

Currently, various efficient algorithms have been developed that could be of interest in the context of underground cables. The authors of [27] evaluated the efficiency of a Cuckoo Search (CS) algorithm based on Taguchi for optimizing the spot welding process. On the other hand, the authors of [28] introduced the Rat Swarm Optimizer (RSO), a new bio-inspired metaheuristic based on natural rat hunting and attacking behaviors. Additionally, the authors of [29] presented a discrete penguin search optimization algorithm (PeSOA) to solve the multiple traveling salesman problem (MTSP).

In various studies, Genetic Algorithms (GA) and Particle Swarm Optimization (PSO) have proven their effectiveness [30–40]. However, PSO stands out in engineering and sciences due to its adaptability, simple structure, fast convergence, ease of implementation, and having fewer parameters, positioning it as a versatile algorithm with superior performance compared to other heuristic algorithms [31,32,34,35].

Despite these advances, there is no simple and efficient methodology for optimizing the ampacity of underground cables. None of the current approaches have addressed this optimization by combining PSO with improvements in implementation, such as an adaptive penalty function to manage physical and economic constraints, adaptive restart strategies, and parameter self-adaptation. Additionally, the lack of consideration for crucial variables such as mutual heating between cables [41] and the absence of sensitivity analysis regarding fluctuating parameters based on climate and soil geography are highlighted.

This study proposes an innovative contribution by addressing these limitations. We will present a mathematical formulation for optimizing ampacity in underground cables. Our proposal integrates the PSO algorithm with substantial improvements in implementation, including an adaptive penalty function, adaptive restart strategies, and parameter self-adaptation. Furthermore, the research will focus on a comparative evaluation with

traditional MATLAB PSO, aiming to improve ampacity by adjusting the dimensions of the thermal backfill without increasing the cross-sectional area of the cable core. Through this research, we seek not only to optimize transmission efficiency but also to advance the understanding of the complexities associated with improvements in the implementation of the PSO algorithm. We aim to offer more effective and economically viable solutions for the electrical industry, marking a significant step in improving ampacity optimization practices in underground cables.

2. Cable Arrangement and Model

High-voltage underground cables in three-phase connection offer various installation configurations, with trefoil (Figure 1a) and flat (Figure 1b) arrangements being the most common. Each cable arrangement has its own unique advantages and disadvantages. According to the research by Quan et al. [42], the flat configuration, whether with or without thermal backfill, exhibits lower temperature rise compared to the trefoil arrangement. This phenomenon is attributed to the fact that in the trefoil arrangement, adjacent cables touching each other increase the temperature of the insulation due to internal conduction, leading to a decrease in their lifespan. The preference for the flat installation in this study is based on this thermal difference, highlighting its superior thermal performance and, consequently, greater operational reliability in the system.

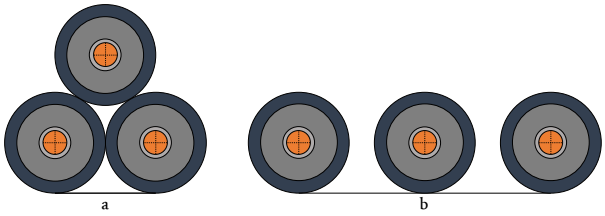

Figure 1. Types of underground cable installation in three-phase transmission lines. (**a**) Trifoil formation, and (**b**) Flat formation.

The use of backfill has a significant effect in reducing temperature in the underground electrical cable system. To achieve effective heat transfer from the cables, natural soil is generally replaced by a thermal backfill with a relatively low thermal resistivity, less than 1.0 K·m/W [1,2].

In Figure 2, the installation method with regular transposition and arrangement of cables, along with all relevant variables for the optimization problem, is shown. Additionally, a segmented conductor cable model (see Figure 3) is used to minimize skin and proximity effects in conductors with large cross-sections [43]. The thermal and electrical parameters of the cable are detailed in Table 1, based on manufacturer specifications [44].

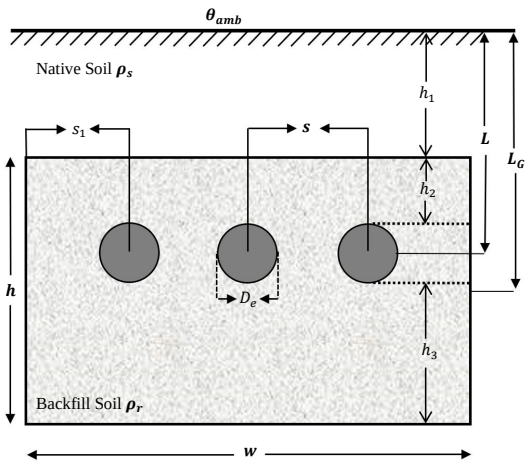

Figure 2. Underground XLPE single-core cables in a flat arrangement and buried in thermal backfill.

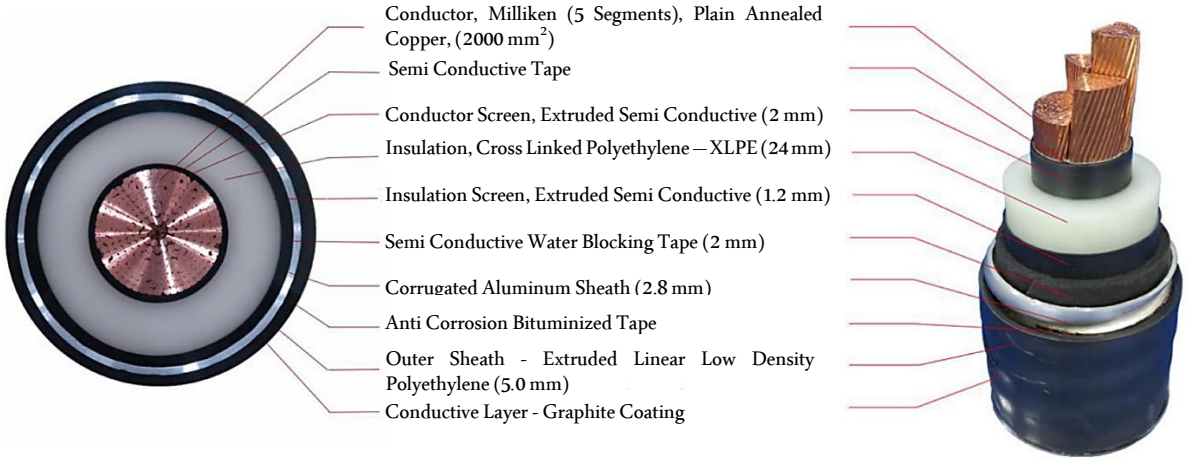

Figure 3. Cross-sectional view of the 220 kV XLPE insulated cable [44].

Table 1. Parameters and specifications of 220 kV XLPE cable [44].

Description	Symbol and Unit	220 kV Cable
Conductor		Milliken—5 seg. Cu
conductor cross section	S (mm^2)	2000 RSM
conductor diameter	d_c (mm)	54.5
semiconductor screen thickness	t_{cs} (mm)	3.5
Insulation		
insulation thickness	t_i (mm)	24.0
insulation outer diameter	D_i (mm)	107.1
Sheath		
aluminum sheath thickness	t_s (mm)	2.8
sheath outer diameter	D_s (mm)	137.4
Outer covering		
outer covering thickness	t_{ce} (mm)	5.0
cable outer diameter	D_e (mm)	147.7
Physical parameters		
maximum conductor temperature	θ_{max} (°C)	90
fundamental frequency	f (Hz)	60
dielectric constant of the insulation	ϵ	2.3
insulation loss factor	tanδ	0.001
conductor resistance at 20 °C	$R_{20}(\Omega/km)$	0.0090
proximity effect constant	k_p	0.37
constant skin effect	k_s	0.435
temperature coefficient of Cu	α_{20}	3.09×10^{-3}
temperature coefficient of Al		4.03×10^{-3}
nominal voltage—phase to phase	U_0 (kV)	220

RMS: Round Multiwire Segmented conductor (Milliken construction).

The cable depicted is a segmented compacted copper conductor, with a screen made of extruded semiconductor. The insulation of the cable is made of a high-quality dry-cured XLPE compound, which is resistant to heat, moisture, and abrasion. The insulation is shielded by a semiconductor tape that is firmly adhered to it. Additionally, the outer covering of the cable is composed of a thermoplastic material (such as PVC, PE, or similar materials) that is continuously extruded over the metallic layer or moisture barrier of the cable.

3. Method

3.1. Ampacity Calculation

To understand the ampacity of cables in underground systems, it is crucial to examine the heat generation resulting from the current flow through the conductor. This thermal efficiency, along with the temperature limits of the insulation, is directly related to the cable's ampacity. In the context of underground cables in homogeneous soils, heat transfer occurs primarily through conduction across the cable components and the surrounding soil. When formulating the problem in two dimensions due to the significantly greater length than the cable diameter, heat conduction in the soil is described by the differential equation [2]:

$$\frac{\partial}{\partial x}\left(\frac{1}{\rho}\frac{\partial \theta}{\partial x}\right) + \frac{\partial}{\partial y}\left(\frac{1}{\rho}\frac{\partial \theta}{\partial y}\right) + W_{int} = c\frac{\partial \theta}{\partial t} \tag{1}$$

where ρ is the thermal resistivity in K·m/W, W_{int} is the heat flux generated in J/s, and c is the volumetric heat capacity.

When solving the heat transfer equation for underground cables, the temperature around the cable is estimated—an essential aspect for evaluating compliance with insulation temperature limits and, consequently, determining ampacity.

The solution to this equation allows estimating the cable temperature at any point around it, a crucial factor in evaluating compliance with insulation temperature limits and, consequently, determining cable ampacity. Two methods are employed to solve Equation (1): the analytical method, providing exact solutions in closed mathematical form, and the numerical method [7]. While the analytical method, though precise, has limitations for complex and realistic problems, especially when the geometry of the arrangement of underground cables is complicated. In contrast, the numerical method, although requiring iterations for approximate solutions, offers flexibility to analyze complex cable systems and apply more realistic boundary conditions. A practical solution to the heat dissipation problem leverages the fundamental similarity between heat flow due to the temperature difference between the conductor and its surroundings and the flow of electric current caused by a potential difference [2]. Given the complexity of the ampacity problem, the solution proposed by Neher and McGrath in 1957 remains foundational, forming the basis for IEEE and IEC standards [3].

Figure 4 presents the thermo-electric equivalence network of the cable and its surroundings. In this representation, the losses in the conductor, corrugated aluminum sheath, and dielectric are denoted as W_c, W_s, and W_d (W/m), respectively. Additionally, the thermal resistances per unit length, T_1, T_2, and T_3 (K·m/W), are shown, corresponding to the thermal resistance of the insulation layer, the thermal resistance of the cable's outer sheath, and the thermal resistance between the cable surface and the surrounding medium.

In the specific case of a cable with corrugated aluminum sheath (with an armor loss factor $\lambda_2 = 0$), the losses can be expressed by the following equation [2,45]:

$$W_T = W_c + W_s + W_d = W_c(1 + \lambda_1) \tag{2}$$

where λ_1, the sheath loss factor, is defined as the ratio of the total losses in the metallic sheath to the total losses in the conductor.

In practice, non-conductive layers of the cable, such as insulation and the separating cover, impede the heat flow from the cables. These layers generally have a cylindrical shape. If we consider a constant thermal resistivity ρ and the inner and outer radii of a layer as r_1 and r_2, respectively, the thermal resistance of a cylindrical layer per unit length can be calculated using the reference [5].

$$T = \frac{\rho}{2\pi}\ln\frac{r_2}{r_1} \tag{3}$$

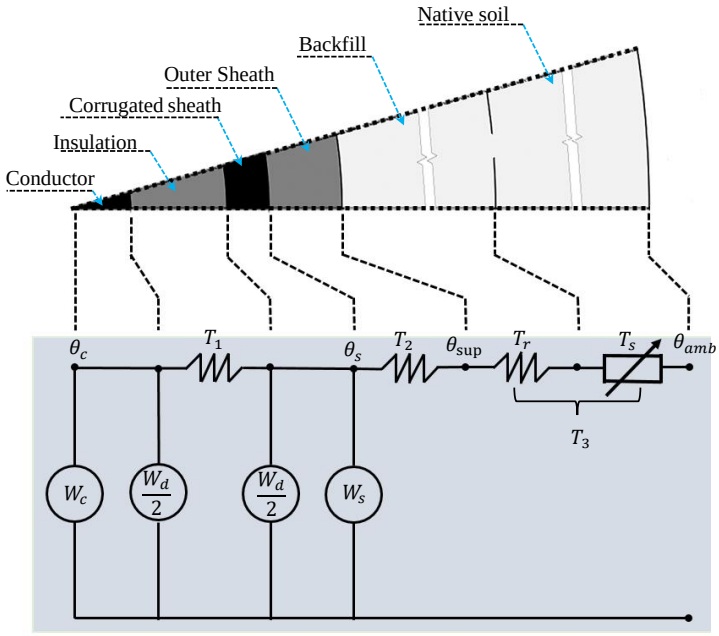

Figure 4. Thermo-electric equivalence network model for underground cable.

The thermal resistance of the metallic parts of the cable, although not equal to zero, is often negligible in ampacity calculations [46]. Ampacity is determined by considering the calculation of temperature-dependent conductor loss $W_c = I^2R$, and we obtain:

$$I = \sqrt{\frac{\Delta\theta - W_d[0.5T_1 + n(T_2 + T_3)]}{R_{ac}[T_1 + n(1 + \lambda_1)(T_2 + T_3)]}} \tag{4}$$

where $\Delta\theta$ is the allowed temperature rise of the cable conductor above the ambient temperature. n denotes the number of conductors in the cable. The dielectric loss (W_d) and the alternating current electrical resistance (R_{ac}) of the metallic parts of the cable are calculated using the corresponding equations:

$$W_d = 2\pi f C U_0^2 tan\delta \qquad R_{ac} = R_{dc}(1 + y_s + y_p) \qquad R_{dc} = \frac{\rho_{20} l}{A}[1 + \alpha_{20}(\theta_c - 20)] \tag{5}$$

where:

$$y_p = \frac{x_p^4}{192 + 0.8x_p^4}\left(\frac{d_c}{s}\right)^2\left[0.312\left(\frac{d_c}{s}\right)^2 + \frac{1.18}{\frac{x_p^4}{192+0.8x_p^4} + 0.27}\right]$$

$$y_s = \frac{x_s^4}{192 + 0.8x_s^4}, \qquad x_p^2 = \frac{8\omega f 10^{-7}}{R_{dc}}k_p \qquad x_s^2 = \frac{8\omega f 10^{-7}}{R_{dc}}k_s$$

The correction factors for the proximity effect (k_p) and the skin effect (k_s) vary depending on the type of cable, as detailed in references [1,12]. Additionally, the parameter λ_1, highlighted as one of the most relevant and effective, is influenced by the backfill dimensions, the distance between cables (s), and the cable model with corrugated sheath [40]. This loss factor (λ_1) consists of losses due to circulating currents (λ_1') and Foucault currents (λ_1'') [3,47]. For three single-core cables, as illustrated in Figure 2, the loss factor due to Foucault currents is calculated as follows [2]:

$$\lambda_1' = \lambda_1' + \lambda_1'' \tag{6}$$

3.2. Thermal External Resistance

When the burial depth of the cable (L) significantly exceeds its external diameter (D_e) in soil with resistivity ρ, the thermal resistance of the surrounding medium can be calculated using Equation (3), replacing r_2 with $4L$ and r_1 with D_e. To enhance heat dissipation in buried cables, it is common to replace part of the native soil around the cables with a thermal backfill material [15]. This is because the external thermal resistance contributes to over 70% of the temperature rise in the conductor of buried cables [2,14]. In practice, high-voltage cables are often placed in backfill material to improve heat dissipation and reduce thermal resistance. Figure 2 illustrates cables arranged on backfill, and the external thermal resistance is described by the following equation [2]:

$$T_3 = \frac{\rho_r}{2\pi}\ln\left\{\left(u + \sqrt{u^2 - 1}\right).F\right\} + \frac{N}{2\pi}(\rho_s - \rho_r)G_b \tag{7}$$

where N is the number of cables in the backfill envelope, and L_G represents the depth of the center of the rectangular backfill measured from the ground surface. The geometric factor G_b encompasses all design parameters through the values of L_G and the equivalent radius r_b. This concept was initially introduced in [5] as an integral part of backfill analysis.

$$u_b = \frac{L_G}{r_b} \quad u = \frac{2L}{D_e} \quad G_b = \ln\left(u_b + \sqrt{u_b^2 - 1}\right) \approx \ln\frac{2L_G}{r_b}$$

For a single-core cable buried under an isothermal plane, the factor F represents the mutual heating effect of other cables in a system with equal load, and for cable p, it is expressed as:

$$F = \prod_{i=1}^{n}\left(\frac{d'_{pi}}{d_{pi}}\right) = \left(\frac{d'_{p1}}{d_{p1}}\right)\left(\frac{d'_{p2}}{d_{p2}}\right)\cdots\left(\frac{d'_{pk}}{d_{pk}}\right)\cdots\left(\frac{d'_{pq}}{d_{pq}}\right) \tag{8}$$

d_{pi} and d'_{pi} cable distances and fictitious images shown in Figure 5.

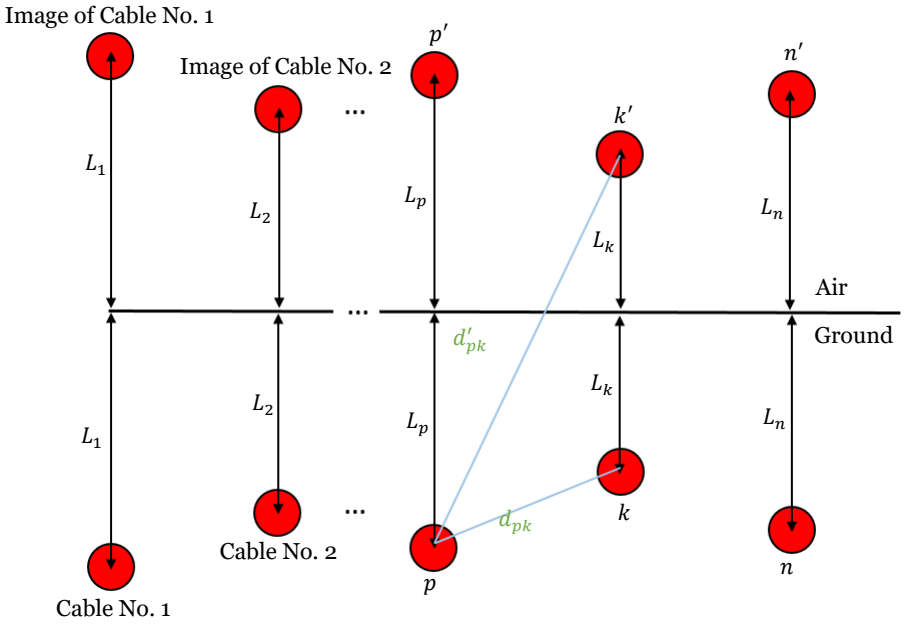

Figure 5. Arrangement of cables and their images on an isothermal plane for the calculation of the *F*-factor.

4. Development of the Proposed Approach

The innovation of this article lies in the presentation of an advanced algorithm designed to optimize the ampacity of underground cables specifically allocated in the backfill. This pioneering approach accurately addresses the challenges associated with determining

the optimal dimensions of the trench, thermal backfill, and cable ampacity, especially in unfavorable environments for high-voltage transmission, considering comprehensively economic and physical installation constraints.

4.1. Formulation of the Objective Function

Equations (4) and (7) are directly influenced by the characteristics of the backfill and the thermal conductivity properties of the soil. Some parameters, such as the thermal resistivity of the soil and ambient temperature, are inherently random, fluctuating along the cable route due to climatic and seasonal variations. In this study, we will assume these parameters to be constants.

In the evolutionary metaheuristic algorithms community, various approaches have been proposed, with the use of penalty functions being the most common. However, these functions have drawbacks, such as the need to adjust multiple parameters, complicating the search for the optimal combination [48,49]. Additionally, solution exploration can be slow, with no guarantee of reaching the optimal solution. To overcome these limitations, modifications to algorithms have been made by introducing the concept of parameter-free penalty functions [48,50,51]. These penalty strategies play a crucial role in balancing the optimization of the objective function and compliance with constraints. In our research, we specifically evaluate adaptive penalization, focusing on the penalty function given by

$$F(\mathbf{x}) = I(\mathbf{x}) + \lambda \sum_{j=1}^{J} g_j(\mathbf{x}) \tag{9}$$

The introduction of the penalization parameter λ (a significantly large number) aims to ensure that the violation of the constraint $g_i(x)$ is of a similar order of magnitude to the value of the objective function $I(x)$. In the case of equality constraints, it is commonly addressed by converting them into approximations of inequality constraints, following the form $g_{(i+k)}(x) \approx h_k(x) - \delta \leq 0$. This implies an increase in the total number of inequality constraints to $j = q + m$, where q is the initial number of inequality constraints, and m is the number of equality constraints. Therefore, the term q in Equation (9) is replaced by j to incorporate both inequality and equality constraints.

4.2. Formulation of Constraints

The design variables include the determination of various parameters, such as the depth of the backfill center (L_G), cable depth (L), spacing between cables (s), backfill width, and thickness (w, h), among others.

With the aim of achieving the optimal configuration and maximizing ampacity, the economic constraint of backfill and installation cost is incorporated as a crucial factor in the optimization method. Additionally, there are physical installation constraints that must be considered in the objective function and are expressed through the following equation:

$$\begin{aligned} C = 30w \cdot L_G + 43.5(w \cdot h - \frac{3}{4}\pi D_e^2) &\leq C_1 \\ s_1 &\geq 0.3 \\ 0.6 \leq h &\leq w \\ L &\geq 0.5 \\ w &\geq 2s_1 + 2s \\ h_1 = L_G - \frac{h}{2} &\geq 0.2 \\ 1.3 \leq h_1 + h_2 + h_3 + D_e = L_G + \frac{h}{2} &\leq 3 \end{aligned} \tag{10}$$

where the cost function C is calculated using the cost parameter values listed in Table 2 and the information presented in Figure 2. It is important to note that the total cost should not exceed the budget C_1, and physical and design limits are imposed on variables, as

illustrated in Figure 2 and detailed in Table 3. The lower limit is determined by physical conditions, while the upper limit is constrained by the cost of backfill material in the optimization process [2,45]. Additionally, the ampacity constraint is simply expressed as $I \geq I_{\text{Load}}$.

Table 2. Cost parameters for the fill optimization [16,45,52].

Task	Base Cost	Term Cost
Excavation	$\$16.5/\text{m}^3$	$w.L_G + w.\frac{h}{2}$
Remove the earth	$\$13.15/\text{m}^3$	$w.L_G + w.\frac{h}{2}$
Backfill with thermal sand	$\$28.5/\text{m}^3$	$w.h - (3/4)\pi D_e^2$

Table 3. Limits of the design variables.

Variable	Lower Limit (m)	Limite Superior (m)
$x_1 = L$	0.5	2
$x_2 = L_G$	0.6	4
$x_3 = w$	1.2	4
$x_4 = h$	0.6	3
$x_5 = s$	$D_e \approx 0.147$	2
$x_6 = s_1$	0.3	2

4.3. Optimization Technique

Stochastic metaheuristics, such as GA and PSO [30,53,54], are preferred in real-world applications due to their mathematical simplicity, ability to address large-scale problems [31,55], and capability to achieve globally optimal solutions in short times [56]. Over time, PSO has demonstrated outstanding performance in areas such as networks, robotics, and power generation, standing out among other nature-inspired algorithms, such as Simulated Annealing (SA), GA, Differential Evolution, Firefly, and Cuckoo. Its distinctive ability to combine local and global search, adaptability, simple structure, fast convergence, ease of implementation, and fewer parameters, along with its widespread acceptance in various fields, position it as a versatile algorithm with superior performance [31,32,34,35].

In various current applications, PSO has shown success by adapting to specific problematics. For example, it has been used to optimize generation scheduling in hybrid renewable energy systems, reducing operational costs [33]. It has also excelled in the optimization of Brayton cycles with solar technologies and dual regenerative systems, effectively achieving irreversibility minimization [36]. In other areas, such as sEMG signal detection and the identification of optimal parameter sets for solar water heaters, PSO has demonstrated precision and effectiveness [37,38]. Additionally, [57] proposes the use of Enhanced Particle Swarm Optimization (EPSO) to minimize energy losses in electrical networks, overcoming the limitations of conventional PSO, while [58] introduces a novel variant, PSO_ML-FSSO, for the Maximum Power Point Tracking (MPPT) task in photovoltaic solar systems, surpassing other known methods in efficiency and settling time.

Recently, there has been a growing interest in hybridizing PSO with other algorithms, such as Discrete Cuckoo Search Particle Swarm Optimization (DCSPSO) [59], and the combination approach of Firefly and PSO (FFA–PSO) to enhance the stability of microgrids [60]. Additionally, the authors of [61] explored the impact of process factors, such as the methanol-oil ratio, ultrasonic power, reaction temperature, reaction time, and pulse frequency, on biodiesel performance using an RSM-GA-PSO hybrid optimization approach. Although these hybrid approaches offer advantages, their computational complexity sometimes poses challenges.

Despite advances in the literature, a gap is identified in the implementation of PSO algorithms that integrate dynamic parameter adaptation and adaptive restart. These features are crucial for stabilizing the algorithm, improving both exploration and exploitation of solutions in the search space.

The PSO algorithm begins its execution by generating random solutions called particles. The population is represented as $\mathbf{X} = [\mathbf{X}_1, \mathbf{X}_2, \mathbf{X}_3, ..., \mathbf{X}_N]^T$, where N indicates the population size, and T denotes transposition. Each particle $\mathbf{X}i(i = 1, 2, ..., N)$ represents an individual in the population and is described as $\mathbf{X}_i(X_{i1}, X_{i2}, X_{i3}, ..., X_{iD})$, with D being the dimension of the search space.

PSO relies on individual experience (Pbest), collective experience (Gbest), and the current movement of particles to determine their next positions in the search space. Experiences are incorporated through two acceleration factors (c_1 and c_2) and two random numbers generated in the interval [0,1]. Simultaneously, the current movement is modulated by an inertia factor (w), whose value varies between $w_{\min}$ and $w_{\max}$. The initial velocity of the population is represented as $\mathbf{V} = [\mathbf{V}_1, \mathbf{V}_2, \mathbf{V}_3, ..., \mathbf{V}_N]^T$. Therefore, the velocity of each particle $\mathbf{X}_i$ is calculated as $\mathbf{V}_i(V_{i1}, V_{i2}, V_{i3}, ..., V_{iD})$.

The following pseudocode presents an adapted version of the PSO algorithm for the optimization of underground cables. Two key elements are highlighted: dynamic parameter adaptation and adaptive restart. The fundamental steps of the proposed PSO algorithm are summarized in Algorithm 1.

Algorithm 1 Fundamental Steps of the Proposed PSO

1. Set PSO Parameters:
   - *nPop*, *reset_prob*, $w_{\min}$, $w_{\max}$, $c1_{\min}$, $c1_{\max}$, $c2_{\min}$, $c2_{\max}$, *MaxIter*, *nvars*, and *VarSize*.
2. Population Initialization:
   - Initialize *adaptive_params* to true (`true`).
3. Initialization:
   - For each particle i in the population:
     - Initialize the position $\mathbf{X}_i$ and velocity $\mathbf{V}_i$ randomly within the defined limits.
     - Initialize the personal best position $\mathbf{Pbest}_i$ and its best fitness $F_{\text{best},i}$ as the initial positions and fitness.
     - Calculate the fitness of the particle $F_i = \text{objective\_function}(\mathbf{X}_i)$.
     - If F_i is better than the global best fitness $F_{\text{best, global}}$, update **Gbest** and $F_{\text{best, global}}$.
4. Iterations:
   - For each iteration up to *MaxIter*:
     - For each particle i in the population:
       - If the adaptive reset condition is met:
         - Reset the particle's position randomly within the limits.
         - Update the velocity and fitness of the particle.
       - Dynamically update the parameter P, where P can represent w, $c1$, and $c2$, with corresponding values for each parameter.
         $$P(k) = P_{\max} + (P_{\min} - P_{\max}) \cdot \left(\frac{k}{\text{MaxIter}}\right)$$
       - Calculate the new velocity of the particle using the standard PSO update formula:
         $$\mathbf{V}_i^{k+1} = w\mathbf{V}_i^k + c1 \cdot \text{rand}() \cdot (\mathbf{Pbest}_i - \mathbf{X}_i) + c2 \cdot \text{rand}() \cdot (\mathbf{Gbest} - \mathbf{X}_i)$$
       - Update the particle's position and apply domain constraints:
         $$\mathbf{X}_i^{k+1} = \text{clip}(\mathbf{X}_i^k + \mathbf{V}_i^{k+1}, \text{VarMin}, \text{VarMax})$$
       - Update the fitness of the particle: $F_i^{k+1} = \text{objective\_function}(\mathbf{X}_i^{k+1})$.
       - Update $\mathbf{Pbest}_i$ and $F_{\text{best},i}$ if F_i^{k+1} is better.
       - Update **Gbest** and $F_{\text{best, global}}$ if F_i^{k+1} is better.
     - Store the best global fitness at each iteration.
5. End.

In the provided pseudocode, the objective function with autoadaptive penalization is implemented using Equation (9), where $g_j(\mathbf{x})$ is defined according to Equation (10) and takes the form $g_j(\mathbf{x}) \leq 0$. Significant penalties have been integrated into the objective function, proportional to the magnitude of constraint violations, resulting in a high penalty

(10^7) for each violated constraint. During the dynamic adaptation of parameters, the update of particle velocities and positions is performed, followed by the evaluation of fitness with penalization. In this process, $f(\mathbf{X}_i^{k+1})$ represents the objective function with incorporated penalization. The code ensures that solutions generated during optimization comply with the problem's constraints by applying penalties when necessary. This strategy strongly encourages the PSO algorithm to converge towards feasible solutions that satisfy the established constraints. The adjusted objective function is evaluated in each iteration of the PSO algorithm, thereby contributing to the efficient search for optimal solutions in the design space.

To enhance understanding of the implemented optimization process, a detailed flowchart has been created and is shown in Figure 6. This diagram illustrates the sequence of steps in the algorithm, starting from the configuration of initial parameters to the evaluation of particle fitness using the autoadaptive penalized objective function, known as the "fitness function". This visual representation provides a clear and concise overview of the optimization algorithm's workflow.

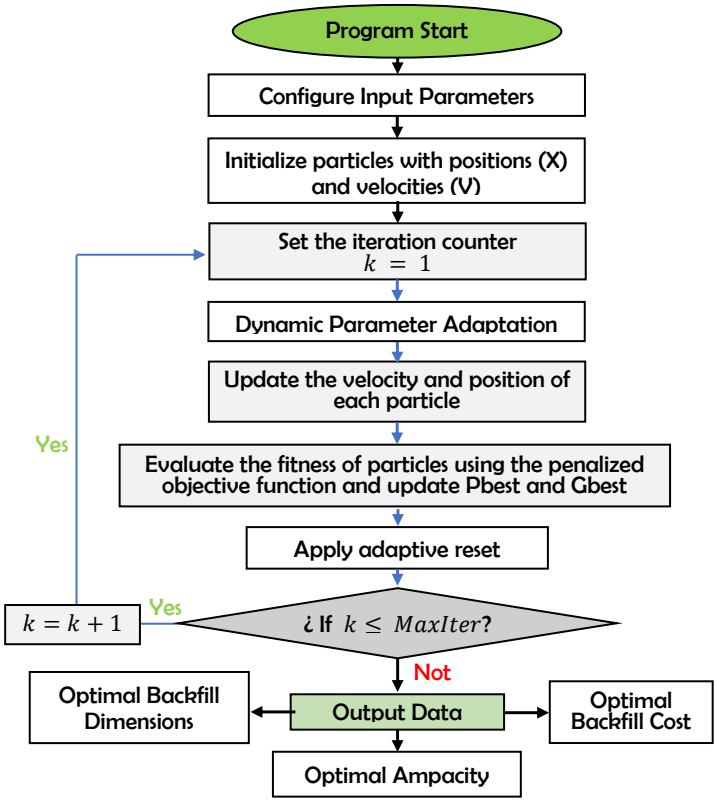

Figure 6. Flowchart of the proposed algorithms.

5. Simulation Results

The proposed method was evaluated on the cable system shown in Figure 2, based on the cable type illustrated in Figure 3. Design variables were constrained to a specific range detailed in Table 3. An upper limit of USD 300 was set for the installation cost (C_1). Constant parameters, such as the thermal resistivity of native soil under normal conditions ($\rho_s = 2.5$ K·m/W), backfill thermal resistivity ($\rho_r = 0.5$ K·m/W), and ambient temperature ($\theta_{amb} = 25$ °C), were obtained from [45].

The proposed optimization problem, defined by Equation (9) and its constraints in Equation (10), was addressed using two approaches: traditional MATLAB PSO (version R2016a, 9.0.0.341360) and the proposed PSO. While traditional PSO is widely used and executed through "particleswarm", requiring manual parameter adjustments, unlike our proposed PSO meticulously tailored for underground cable ampacity optimization. The

proposed version incorporates dynamic parameter adaptation and adaptive restart, improves the stopping criterion, and was evaluated alongside traditional PSO under penalty functions for a fair comparison. All tests were conducted in MATLAB R2016a, using an Intel(R) Core(TM) i7-8750H CPU @ 2.20 GHz, 2.21 GHz, with 12.00 GB of RAM. This study highlights the distinctive features of the proposed PSO, supporting its utility and emphasizing its significant improvement over traditional PSO in exploring the search space.

The PSO algorithm parameters were carefully selected: a population of 100, inertial weight (w) from 1 to 0.1, modified acceleration coefficients (c_1 and c_2) from 2 to 1. An adaptive restart strategy with a 2% probability at each iteration was implemented to encourage exploration. These specific values are chosen to enhance the convergence and efficiency of the PSO algorithm in ampacity optimization.

Three independent runs of the proposed PSO algorithm and the traditional PSO were conducted, as depicted in Figure 7. The proposed PSO (Figure 7a) stands out for its rapid convergence, achieving the goal in 30 iterations, in contrast to the 200 iterations of the traditional MATLAB PSO (Figure 7b). This efficiency suggests a higher exploitation capacity, swiftly focusing on promising solutions. Additionally, both algorithms exhibit notable stability over time, as solutions show no significant improvements. This indicates that both algorithms converge towards an optimal solution more quickly in fewer iterations. Furthermore, in the figures, a slight variability in the convergence for the proposed algorithm is observed, with higher variability for the traditional PSO, attributable to its stochastic nature.

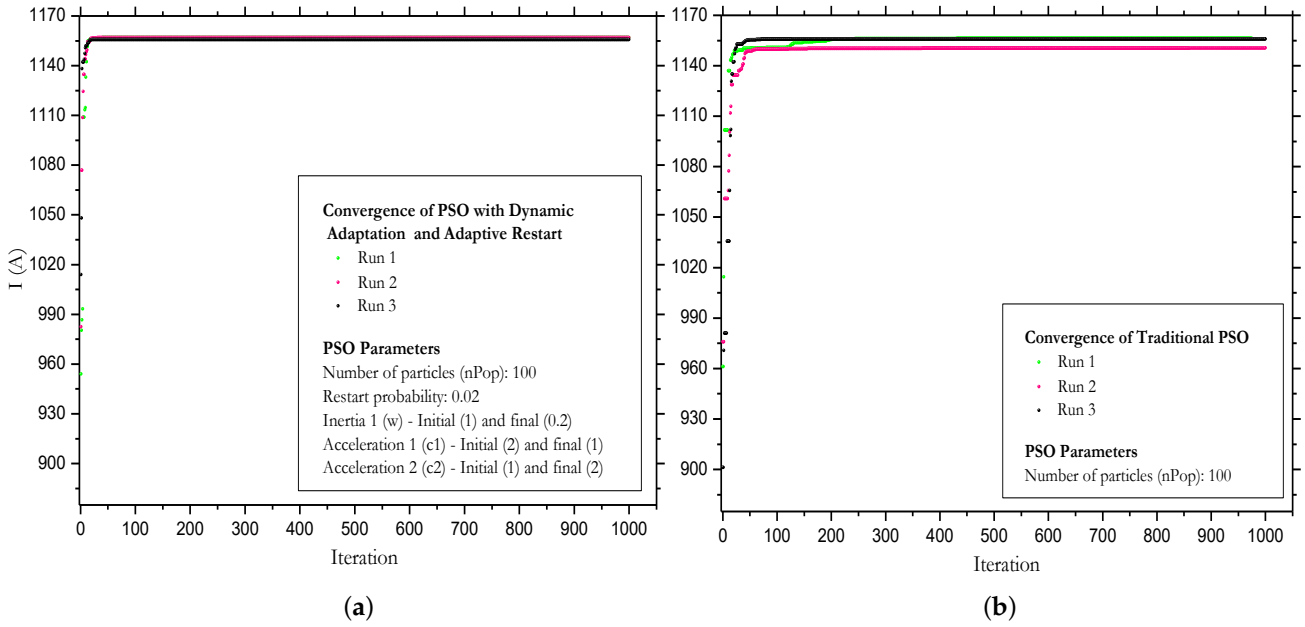

Figure 7. Characteristic Convergence of PSO for Ampacity Maximization. (**a**) Proposed PSO, and (**b**) Traditional PSO.

The enhanced implementation of the proposed algorithm, featuring dynamic adaptation and adaptive restart, contributes to stability and coherence by reducing fluctuations and enhancing convergence. Adaptive restart, strategically restarting particles, generates consistent and reliable results across various executions. Without these improvements, results tend to be more unstable. The effectiveness of dynamic adaptation and restart depends on the problem, making multiple runs and statistical analyses crucial for robust performance evaluation.

To assess performance, each algorithm was executed 1000 times. The optimal results, recorded for cable ampacity in each run, are visually presented in Figures 8a and 9a. Additionally, algorithm performances are detailed in Table 4, providing crucial information such as the best ampacity value, average, and standard deviation, among other relevant aspects.

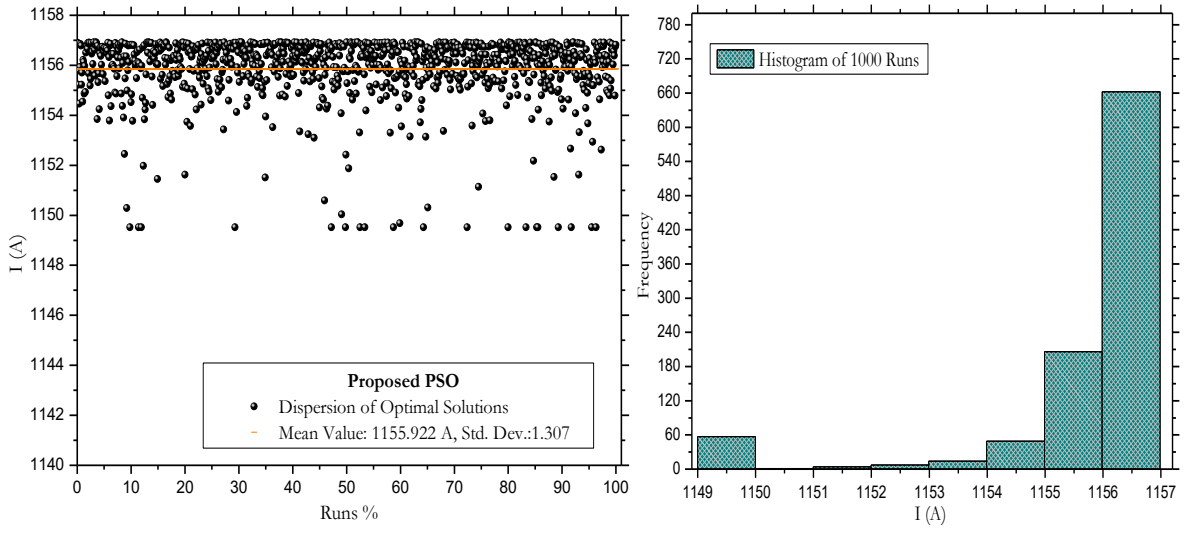

(**a**) (**b**)

Figure 8. (**a**) Dispersion and (**b**) histogram of optimal ampacity with proposed PSO.

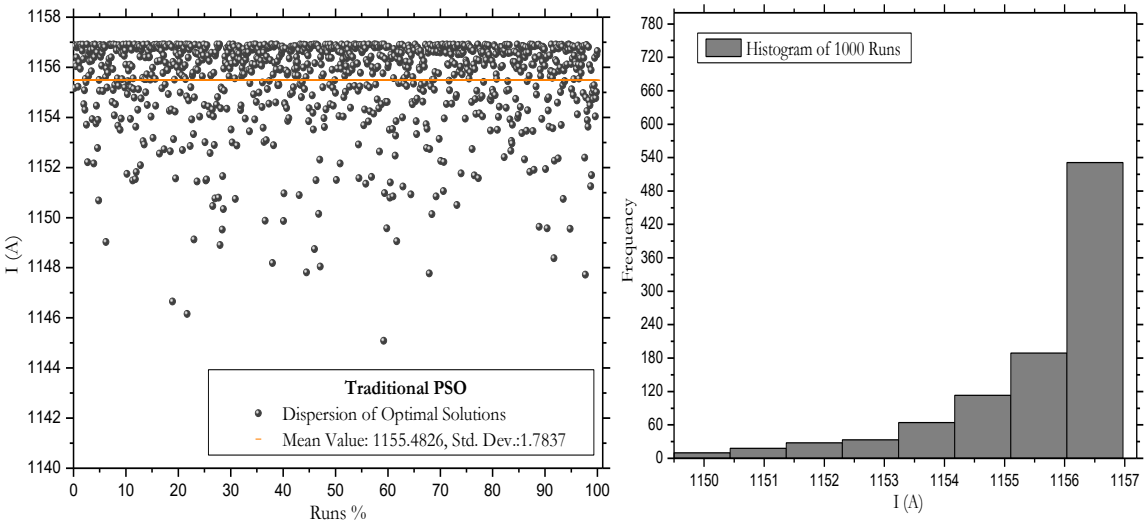

(**a**) (**b**)

Figure 9. (**a**) Dispersion and (**b**). histogram of optimal ampacity with traditional PSO.

Table 4. Performance results of algorithms in 1000 runs.

Performance Metrics	Proposed PSO	Traditional PSO
Best solution	1156.9150	1156.9107
Peor solución	1149.5165	1145.0845
Range of variation	7.3985	11.8263
Mean value	1155.9221	1155.4815
Standard deviation	1.3071	1.7837
Success Probability	66.10%	56.40%

When comparing results between the proposed PSO algorithm and the traditional PSO, notable differences in terms of accuracy, performance, and consistency are highlighted. The histogram analysis in Figures 8b and 9b reveals that the maximum value is most frequently recorded in the range of 1156 to 1157 A. The success probability for this interval is 66.1% in the proposed PSO and 56.4% in the traditional PSO, respectively. Although traditional PSO is 81% faster, the proposed PSO stands out for its accuracy. Despite being slower, its precise approach makes it ideal when accuracy is crucial. Additionally, its simplicity and clarity

facilitate understanding and adjustment, being accessible with fewer parameters than the traditional approach. The introduction of restart probabilities and dynamic adaptation enhances the exploration of the search space, achieving more efficient convergences. This code is a valuable tool for intuitively and effectively addressing optimization problems.

Based on these comparisons and analyses, the proposed algorithm is selected as the most suitable, effective, and reliable for conducting comparisons in cable ampacity optimization with and without backfill. The notable results are presented in Table 5.

Table 5. Optimization result.

Backfill Dimensions		Parameters and Cost	
Variable (m)	**Values**	**Variable**	**Values**
L	0.500	Total cost ($)	300
L_G	0.872	Backfill cost ($)	94.7
w	3.562	Ampacity BackFill (A)	1156.915
h	1.344	Ampacity Without backfill (A)	969.9
s	1.481	W_d (W/m)	3×3.546
λ_1	2.667	W_I (W/m)	3×17.67

Initially, the cable ampacity without considering backfill is 980.883 A. This would imply the need to use a conductor with a larger cross-sectional area to support a load current of 1000 A. However, by applying ampacity optimization considering the backfill configuration, the cable ampacity increases to 1156.9 A, making it suitable for a load current of 1000 A. Therefore, the percentage increase in the ampacity of the cable installed with backfill compared to the cable without backfill is approximately 18.45%. This highlights the benefits of backfill in cable ampacity optimization.

Figure 10 indicates that ampacity is maximum at s = 2.3 m, albeit at a high cost. Below this value, it decreases due to the proximity effect, while above it decreases due to increased thermal resistivity. The increase in backfill volume directly affects the total installation cost, influencing ampacity up to a balance point, beyond which it decreases (Figure 11).

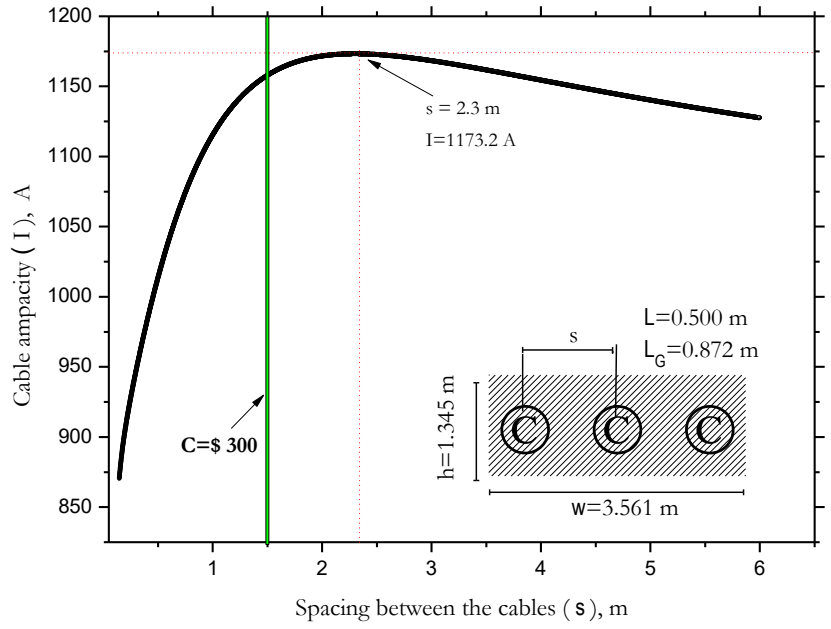

Figure 10. Effect of cable spacing on cable ampacity. In the bottom right corner, the flat formation installation is depicted within the thermal backfill.

It is essential to note that increasing the backfill volume does not guarantee an unlimited increase in ampacity. The proximity effect influences the spacing between cables (s),

and with a constant backfill width (w), current losses decrease due to better dissipation and reduced electrical resistance provided by the backfill. The optimum value of s that maximizes ampacity is reached when both effects balance each other.

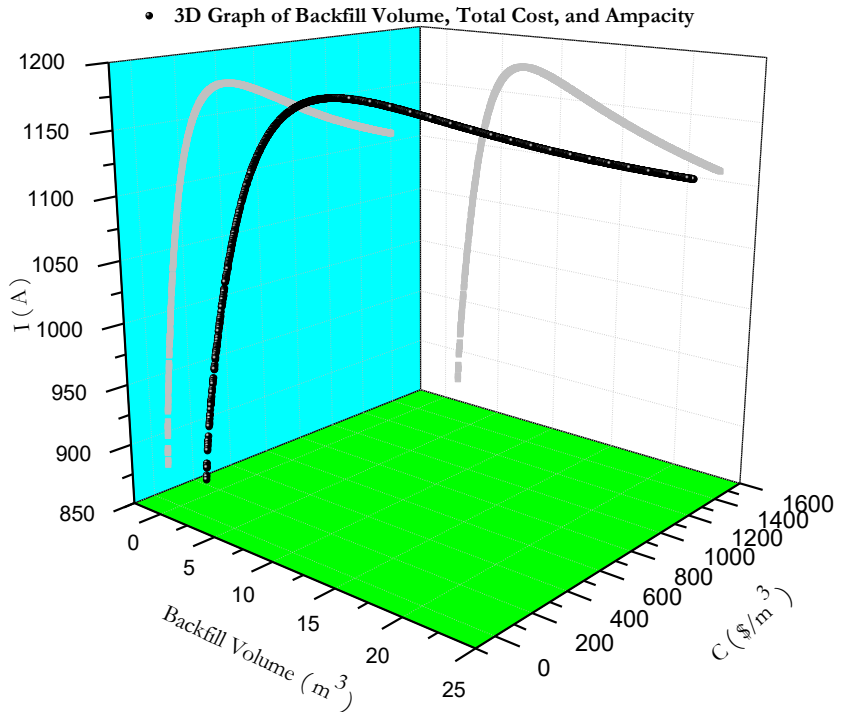

Figure 11. Relationship among Ampacity, Total Cost, and Backfill Volume, Including Their Projections on the Vertical Planes.

Our proposal suggests delaying or avoiding investments in larger-section cables for underground lines, focusing on the use of backfill materials to achieve optimal ampacity at a more favorable cost. Additionally, in places where cables are already overloaded, the addition of backfill could be considered instead of installing larger-section cables.

The ampacity of buried cables is often based on constant values of ρ_s and θ_a. Although relatively high values for these variables are usually assumed, relying on designer estimates and available records, it is essential to note that they may experience unforeseen variations during cable operation, influenced by climatic and geographical changes along the route and during different seasons of the year. It is crucial to consider that these variations directly impact the cable's ampacity. In response to these fluctuations, sensitivity information has been developed to assess cable ampacity, using dimensionless measures represented by S_{ρ_s} and S_θ [2,16].

$$S_{\rho_s} = \frac{\partial I}{\partial \rho_s} \cdot \frac{\rho_s}{I} \qquad S_\theta = \frac{\partial I}{\partial \theta_{\text{amb}}} \cdot \frac{\theta_{\text{amb}}}{I}$$

These sensitivity parameters indicate how the cable's ampacity varies concerning ρ_s and θ_a at the nominal point. To calculate sensitivity coefficients, partial derivatives are taken in Equation (4). In practical designs, both S_{ρ_s} and S_θ are negative, indicating that the cable's ampacity decreases with an increase in ρ_s and θ_a. Sensitivity contours, based on nominal values of $\rho_s = 2.5$ K·m/W, $\theta_{\text{amb}} = 25$ °C, and $I = 1156.915$A (Table 5), reveal an ampacity sensitivity to soil resistivity, $S_\rho = -0.3999$. This value indicates that an increase in the thermal resistivity of the soil by $\Delta\rho_s = 0.5$ K·m/W from the nominal value of 2.5 K·m/W (a 20% percentage variation) will result in a change ΔI_ρ in the allowable cable ampacity, equal to

$$\Delta I_\rho = \frac{I}{\rho_s} \cdot S_\rho \cdot \Delta\rho_s = \frac{1156.915}{2.5} \cdot (-0.3999) \cdot 0.5 = -92.527\,\text{A}$$

resulting in a steady-state ampacity of $1156.915 - 92.527 = 1064.388$ A.

Similarly, the same cable design shows an ampacity sensitivity to ambient temperature of $S_\theta = -0.2037$. That is, an increase of $\Delta\theta_{\text{amb}} = 10$ °C from the nominal value of 25 °C (a 40% percentage variation) will cause a change in the cable's ampacity equal to

$$\Delta I_\theta = \frac{I}{\theta_{\text{amb}}} \cdot S_\theta \cdot \Delta\theta_{\text{amb}} = \frac{1156.915}{25} \cdot (-0.2037) \cdot 10 = -94.28\,\text{A}$$

resulting in an ampacity of $1156.915 - 94.28 = 1062.635$ A.

The choice of the considered variations depends on the context and the desired precision. There is no single correct value, as it can vary depending on the actual magnitude of the variations. In the absence of specific information about variability and with the intention of being conservative, a discussed conservative percentage has been selected in the previous paragraphs.

When the design experiences simultaneous changes in soil thermal resistivity and ambient temperature, the total change in ampacity is calculated as

$$\Delta I = \Delta I_\rho + \Delta I_\theta = -92.527 - 94.28 = -186.80\,\text{A}$$

resulting in a cable ampacity of 970.115 A.

These sensitivity results indicate that variations in parameters significantly impact the cable ampacity, either decreasing or increasing based on positive or negative changes. It is recommended to conduct a sensitivity analysis over a broader range of variations to capture the full impact of simultaneous changes in environmental conditions on cable ampacity. This will provide a more detailed and robust insight for the design of buried cables. Given the variable nature of environmental conditions, a probabilistic approach could be considered in future studies, along with evaluating variations in the cable's cross-sectional area to enhance ampacity. This involves assessing cable ampacity in terms of probability distributions for ρ_s and θ_a in a broader context, offering a more comprehensive understanding of the associated uncertainty.

6. Conclusions

This study has comprehensively addressed the challenge of optimizing the ampacity in 220 kV underground electric cables with XLPE insulation installed in thermal backfill. Our proposal successfully combines the PSO algorithm with significant improvements in implementation, such as an adaptive penalization function, adaptive restart strategies, and parameter self-adaptation. By comparing the results with traditional MATLAB PSO, we have conclusively demonstrated that our approach overcomes limitations associated with result variability and ensures efficiency in searching for the optimal ampacity value and design variables.

The obtained results are promising, highlighting a success probability of 66.1% in finding the optimal ampacity value, contrasting with the traditional approach's 56.4%. Furthermore, we achieved an optimal ampacity of 1156.9 A for the cable with thermal backfill, along with specific dimensions and a cost of \$94.7/m^3. This accomplishment translates into a significant 18.45% increase in ampacity compared to the cable without thermal backfill, confirming the effectiveness of our proposal.

The conducted sensitivity analysis emphasizes the importance of considering factors such as soil thermal resistivity and ambient temperature, which significantly affect cable ampacity. This knowledge provides a solid foundation for addressing variations in environmental conditions and strengthens the robustness of our design.

Moreover, our proposal not only focuses on improving ampacity by adjusting thermal backfill instead of increasing the core cable's cross-sectional area but also on the enhanced implementation of PSO. This technical and efficient perspective offers decision makers in energy systems a valuable and easily implementable tool with potential applications in various areas. As future work, we propose evaluating the simultaneous optimization of

cable cost and ampacity using a probabilistic approach, contributing to advancements in electrical system optimization.

Author Contributions: Conceptualization, B.A.A. and M.T.P.; methodology, B.A.A.; software, B.A.A.; validation, B.A.A.; formal analysis, B.A.A.; investigation, B.A.A. and M.T.P.; resources, B.A.A.; original draft preparation, B.A.A.; writing—review and editing, B.A.A., M.T.P. and D.W.P.; visualization, M.T.P., D.W.P., D.M., E.U. and C.R.; supervision, B.A.A. All authors have read and agreed to the published version of the manuscript.

Funding: This work was carried out as part of my doctoral studies with the support of a scholarship granted by the National Council of Science, Technology, and Technological Innovation (CONCYTEC), which covered the costs of my studies. I appreciate the financial support from CONCYTEC and the National University of Engineering (UNI) for providing me with education. The publication of this article was solely funded by the authors and co-authors, with no direct financial contribution from other entities.

Data Availability Statement: The data presented in this study are contained within the article.

Conflicts of Interest: The authors declare no conflicts of interest.

References

1. Czapp, S.; Ratkowski, F. Optimization of thermal backfill configurations for desired high-voltage power cables ampacity. *Energies* **2021**, *14*, 1452. [CrossRef]
2. Anders, G.J. *Rating of Electric Power Cables in Unfavorable Thermal Environment*; Wiley: Hoboken, NJ, USA, 2005.
3. *IEC 60287-1-1*; Electric Cables—Calculation of the Current Rating—Part 1-1: Current Rating Equations (100% Load Factor) and Calculation of Losses—General; Tech. Rep.; International Electrotechnical Commission: Geneva, Switzerland, 2006.
4. *IEC 60287-2-1*; Electric Cables—Calculation of the Current Rating, Part 2-1: Thermal Resistance—Calculation of Thermal Resistance. International Electrotechnical Commission: Geneva, Switzerland, 2006.
5. Neher, J.H.; McGrath, M.H. The calculation or the temperature rise and load capability of cable systems. *RATIO* **1994**, *50*, 5. [CrossRef]
6. De León, F. Major factors affecting cable ampacity. In Proceedings of the 2006 IEEE Power Engineering Society General Meeting, Montreal, QC, Canada, 18–22 June 2006.
7. De Leon, F. Calculation of underground cable ampacity. In *Wire and Cable Handbook*; The Electricity Forum: Pickering, ON, Canada, 2005.
8. Ratkowski, F.; Kołtun, M.; Czapp, S. The effect of cable duct diameter on the ampacity of high-voltage power cables. *Przegląd Elektrotech.* **2022**, *98*, 141–144. [CrossRef]
9. *ETAP*—Cable Thermal Software. Available online: https://etap.com/es/product/cable-thermal-software (accessed on 1 December 2022).
10. Che, C.; Yan, B.; Fu, C.; Li, G.; Qin, C.; Liu, L. Improvement of cable current carrying capacity using COMSOL software. *Energy Rep.* **2022**, *8*, 931–942. [CrossRef]
11. Al-Saud, M.S.; El-Kady, M.A.; Findlay, R.D. A new approach to underground cable performance assessment. *Electr. Power Syst. Res.* **2008**, *78*, 907–918. [CrossRef]
12. Benato, R.; Colla, L.; Sessa, S.D.; Marelli, M. Review of high current rating insulated cable solutions. *Electr. Power Syst. Res.* **2016**, *133*, 36–41. [CrossRef]
13. Williams, J.A.; Parmar, D.; Conroy, M.W. Controlled backfill optimization to achieve high ampacities on transmission cables. *IEEE Trans. Power Deliv.* **1994**, *9*, 544–552. [CrossRef]
14. De León, F.; Anders, G.J. Effects of backfilling on cable ampacity analyzed with the finite element method. *IEEE Trans. Power Deliv.* **2008**, *23*, 537–543. [CrossRef]
15. Saleeby, K.E.; Black, W.Z.; Hartley, J.G. Effective thermal resistivity for power cables buried in thermal backfill. *IEEE Trans. Power Appar. Syst.* **1979**, *6*, 2201–2214. [CrossRef]
16. El-Kady, M.A. Optimization of power cable and thermal backfill configurations. *IEEE Trans. Power Appar. Syst.* **1982**, *12*, 4681–4688. [CrossRef]
17. Klimenta, D.O.; Perovic, B.D.; Jevtic, M.D.; Radosavljevic, J.N.; Arsic, N.B. Thermal FEM-based procedure for design of energy-efficient underground cable lines. *Univ. Sci. J.* **2014**, *10*, 162–188.
18. Cichy, A.; Sakowicz, B.; Kaminski, M. Economic optimization of an underground power cable installation. *IEEE Trans. Power Deliv.* **2017**, *33*, 1124–1133. [CrossRef]
19. Zarchi, D.A.; Vahidi, B.; Haji, M.M. Optimal configuration of underground cables to maximise total ampacity considering current harmonics. *IET Gener. Transm. Distrib.* **2014**, *8*, 1090–1097. [CrossRef]
20. Nahman, J.; Tanaskovic, M. Calculation of the loading capacity of high voltage cables laid in close proximity to heat pipelines using iterative finite-element method. *Int. J. Electr. Power Energy Syst.* **2018**, *103*, 310–316. [CrossRef]

21. Al-Saud, M.S. PSO of power cable performance in complex surroundings. *IET Gener. Transm. Distrib.* **2018**, *12*, 2452–2461. [CrossRef]
22. Ocłoń, P.; Cisek, P.; Taler, D.; Pilarczyk, M.; Szwarc, T. Optimizing of the underground power cable bedding using momentum-type particle swarm optimization method. *Energy* **2015**, *92*, 230–239. [CrossRef]
23. Ocłoń, P.; Rerak, M.; Rao, R.V.; Cisek, P.; Vallati, A.; Jakubek, D.; Rozegnał, B. Multiobjective optimization of underground power cable systems. *Energy* **2021**, *215*, 119089. [CrossRef]
24. Perović, B.; Klimenta, D.; Tasić, D.; Raičević, N.; Milovanović, M.; Tomović, M.; Vukašinović, J. Increasing the ampacity of underground cable lines by optimising the thermal environment and design parameters for cable crossings. *IET Gener. Transm. Distrib.* **2022**, *16*, 2309–2318. [CrossRef]
25. Wang, J.; Liu, B.; Li, D.; Ma, X.; Zhao, B.; Yang, Z. Research on optimal placement methodology of power cable in ductbank. *Energy Rep.* **2023**, *9*, 46–57. [CrossRef]
26. Fan, D.; Huang, J.; Zhu, Z.; Liang, Y.; Liu, W. High-voltage Cable Arrangement Optimization Design Method. In Proceedings of the 2023 8th Asia Conference on Power and Electrical Engineering (ACPEE), Tianjin, China, 14–16 April 2023; pp. 2561–2567.
27. Chaki, S.; Bose, D. Optimisation of spot-welding process using Taguchi based Cuckoo search algorithm. *Decis. Mak. Appl. Manag. Eng.* **2022**, *5*, 316–328. [CrossRef]
28. Mzili, T.; Riffi, M.E.; Mzili, I.; Dhiman, G. A novel discrete Rat swarm optimization (DRSO) algorithm for solving the traveling salesman problem. *Decis. Mak. Appl. Manag. Eng.* **2022**, *5*, 287–299. [CrossRef]
29. Mzili, I.; Mzili, T.; Riffi, M.E. Efficient routing optimization with discrete penguins search algorithm for MTSP. *Decis. Mak. Appl. Manag. Eng.* **2023**, *6*, 730–743. [CrossRef]
30. Bemani, A.; Xiong, Q.; Baghban, A.; Habibzadeh, S.; Mohammadi, A.H.; Doranehgard, M.H. Modeling of cetane number of biodiesel from fatty acid methyl ester (FAME) information using GA-, PSO-, and HGAPSO-LSSVM models. *Renew. Energy* **2020**, *150*, 924–934. [CrossRef]
31. Nayak, J.; Swapnarekha, H.; Naik, B.; Dhiman, G.; Vimal, S. 25 years of particle swarm optimization: Flourishing voyage of two decades. *Arch. Comput. Methods Eng.* **2023**, *30*, 1663–1725. [CrossRef]
32. Khan, A.; Hizam, H.; bin Abdul Wahab, N.I.; Lutfi Othman, M. Optimal power flow using hybrid firefly and particle swarm optimization algorithm. *PLoS ONE* **2020**, *15*, e0235668. [CrossRef]
33. Wynn, S.L.L.; Boonraksa, T.; Boonraksa, P.; Pinthurat, W.; Marungsri, B. Decentralized Energy Management System in Microgrid Considering Uncertainty and Demand Response. *Electronics* **2023**, *12*, 237. [CrossRef]
34. Dao, S.D. A Note On The Popularity of Stochastic Optimization Algorithms in Different Fields: A Quantitative Analysis from 2007 to 2017. *arXiv* **2019**, arXiv:1907.01453.
35. Haji, V.H.; Monje, C.A. Fractional order fuzzy-PID control of a combined cycle power plant using Particle Swarm Optimization algorithm with an improved dynamic parameters selection. *Appl. Soft Comput.* **2017**, *58*, 256–264. [CrossRef]
36. Oyewola, O.M.; Petinrin, M.O.; Labiran, M.J.; Bello-Ochende, T. Thermodynamic optimisation of solar thermal Brayton cycle models and heat exchangers using particle swarm algorithm. *Ain Shams Eng. J.* **2023**, *14*, 101951. [CrossRef]
37. Alam, S.; Zhao, X.; Niazi, I.K.; Khan, M.A. A comparative analysis of global optimization algorithms for surface electromyographic signal onset detection. *Decis. Anal. J.* **2023**, *8*, 100294. [CrossRef]
38. Mahto, P.K.; Das, P.P.; Diyaley, S.; Kundu, B. Parametric optimization of solar air heaters with dimples on absorber plates using metaheuristic approaches. *Appl. Therm. Eng.* **2024**, *2024*, 122537. [CrossRef]
39. Das, M.; Roy, A.; Maity, S.; Kar, S.; Sengupta, S. Solving fuzzy dynamic ship routing and scheduling problem through new genetic algorithm. *Decis. Mak. Appl. Manag. Eng.* **2022**, *5*, 329–361. [CrossRef]
40. del-Pino-López, J.C.; Cruz-Romero, P.; Serrano-Iribarnegaray, L.; Martínez-Román, J. Magnetic field shielding optimization in underground power cable duct banks. *Electr. Power Syst. Res.* **2014**, *114*, 21–27. [CrossRef]
41. Bravo-Rodríguez, J.C.; del-Pino-López, J.C.; Cruz-Romero, P. A survey on optimization techniques applied to magnetic field mitigation in power systems. *Energies* **2019**, *12*, 1332. [CrossRef]
42. Quan, L.; Fu, C.; Si, W.; Yang, J.; Wang, Q. Numerical study of heat transfer in underground power cable system. *Energy Procedia* **2019**, *158*, 5317–5322. [CrossRef]
43. da Silva, F.F.; Bak, C.L. *Electromagnetic Transients in Power Cables*; Springer: Berlin/Heidelberg, Germany, 2013.
44. 127/220 kv Copper Conductor Xlpe Insulated Corrugated Aluminum Sheath Pvc Sheath Power Cable. 2018. Available online: http://gzny13922732011.voip366.com/ (accessed on 15 April 2023).
45. Shabani, H.; Vahidi, B. A probabilistic approach for optimal power cable ampacity computation by considering uncertainty of parameters and economic constraints. *Int. J. Electr. Power Energy Syst.* **2019**, *106*, 432–443. [CrossRef]
46. Anders, G.J. *Rating of Electric Power Cables: Ampacity Computations for Transmission, Distribution, and Industrial Applications*; IEEE: Piscataway, NJ, USA, 1997.
47. Tong, Q.; Qi, J.; Wang, Y.; Liang, L.; Meng, X.; Zhang, Q. Power cable ampacity and influential factors analysis under operation. *J. Inf. Process. Syst.* **2018**, *14*, 1136–1149.
48. Tessema, B.; Yen, G.G. A self adaptive penalty function based algorithm for constrained optimization. In Proceedings of the 2006 IEEE International Conference on Evolutionary Computation, Vancouver, BC, Canada, 16–21 July 2006; pp. 246–253.
49. Garg, H. A hybrid GSA-GA algorithm for constrained optimization problems. *Inf. Sci.* **2019**, *478*, 499–523. [CrossRef]

50. Deb, K. An efficient constraint handling method for genetic algorithms. *Comput. Methods Appl. Mech. Eng.* **2000**, *186*, 311–338. [CrossRef]
51. Barbosa, H.J.C.; Lemonge, A.C.C. An adaptive penalty scheme in genetic algorithms for constrained optimization problems. In Proceedings of the 4th Annual Conference on Genetic and Evolutionary Computation, New York, NY, USA, 9–13 July 2002; pp. 287–294.
52. Perović, B.D.; Tasić, D.S.; Klimenta, D.O.; Radosavljević, J.N.; Jevtić, M.J.; Milovanović, M.J. Optimising the thermal environment and the ampacity of underground power cables using the gravitational search algorithm. *IET Gener. Transm. Distrib.* **2018**, *12*, 423–430. [CrossRef]
53. Alam, M.N.; Das, B.; Pant, V. A comparative study of metaheuristic optimization approaches for directional overcurrent relays coordination. *Electr. Power Syst. Res.* **2015**, *128*, 39–52. [CrossRef]
54. Garg, H. A hybrid PSO-GA algorithm for constrained optimization problems. *Appl. Math. Comput.* **2016**, *274*, 292–305. [CrossRef]
55. Panda, Dr. Comparing Different Characteristics of Deterministic and Stochastic Optimization Methods. 12 May 2020. Available online: https://learnwithpanda.com/2020/05/12/ (accessed on 15 December 2022).
56. Dao, S.D.; Abhary, K.; Marian, R. An improved structure of genetic algorithms for global optimisation. *Prog. Artif. Intell.* **2016**, *5*, 155–163. [CrossRef]
57. Adegoke, S.A.; Sun, Y.; Wang, Z. Minimization of active power loss using enhanced particle swarm optimization. *Mathematics* **2023**, *11*, 3660. [CrossRef]
58. Kumar, D.; Chauhan, Y.K.; Pandey, A.S.; Srivastava, A.K.; Kumar, V.; Alsaif, F.; Elavarasan, R.M.; Islam, M.R.; Kannadasan, R. A Novel Hybrid MPPT Approach for Solar PV Systems Using Particle-Swarm-Optimization-Trained Machine Learning and Flying Squirrel Search Optimization. *Sustainability* **2023**, *15*, 5575. [CrossRef]
59. Zhang, J.; Liu, X.; Zhang, B. Mathematical modelling and a discrete cuckoo search particle swarm optimization algorithm for mixed model sequencing problem with interval task times. *J. Intell. Manuf.* **2024**. [CrossRef]
60. Lasabi, O.; Swanson, A.; Jarvis, L.; Aluko, A.; Goudarzi, A. Coordinated Hybrid Approach Based on Firefly Algorithm and Particle Swarm Optimization for Distributed Secondary Control and Stability Analysis of Direct Current Microgrids. *Sustainability* **2024**, *16*, 1204. [CrossRef]
61. Ahmad, A.; Yadav, A.K.; Singh, A.; Singh, D.K.; Ağbulut, Ü. A hybrid RSM-GA-PSO approach on optimization of process intensification of linseed biodiesel synthesis using an ultrasonic reactor: Enhancing biodiesel properties and engine characteristics with ternary fuel blends. *Energy* **2024**, *288*, 129077. [CrossRef]